PHYSICAL REVIEW D

PARTICLES AND FIELDS

THIRD SERIES, VOLUME 27, NUMBER 9 1 MAY 1983

Anomalous electron-pair production in 17-GeV/c $\pi^- p$ collisions

M. R. Adams, G. Abshire,* C. Brown,† E. S. Crandall,‡ J. Goldberger, P. D. Grannis, B. T. Meadows,§ and J. Stekas**
State University of New York, Stony Brook, New York 11794

G. J. Donaldson,†† H. A. Gordon, G. R. Morris,‡‡ and P. Rehak
Brookhaven National Laboratory, Upton, New York 11973

L. Cormell
University of Pennsylvania, Philadelphia, Pennsylvania 19104
(Received 19 November 1982)

We have measured inclusive e^+e^- production in 17-GeV/c $\pi^- p$ collisions and find anomalously large cross sections for pair masses below 0.6 GeV/c^2 and Feynman $x < 0.5$. Charged particles and photons produced in association with e^+e^- were measured. Decays of known resonances are not capable of explaining the effect. No excess of photons or charged particles associated with the anomalous pairs is detected. Implications of our results for various models and for direct single-electron and photon production are discussed.

I. INTRODUCTION

Two of the recurrent themes in studies of hadron-hadron collisions over the past decade have been single-lepton and dilepton production. The former emerged as a surprise in 1974 with the reports of lepton-to-pion ratios at the level of 10^{-4} at large p_T.[1] Subsequent work, including studies of charmed-particle production at high energies, has helped to elucidate some of the contributions to single-lepton yields. However, reports of large e/π ratios at low p_T (and sometimes low energy)[2-5] cannot be explained on the basis of known-particle production and decay. The evidence for the low-p_T and low-s single leptons has been challenged by an experiment which reports e/π at small explainable levels.[6] Experiments which have seen anomalous single leptons are consistent with equal rates for e^+ and e^-, thus permitting the possibility of a parent e^+e^- source.

Studies of dilepton production have traditionally been aimed at the discovery and study of massive spin-1 mesons, and also at the massive-dilepton continuum where application of the Drell-Yan mechanism[7] allows study of short-distance interactions of hadronic constituents. In recent years there have been several experiments which have extended the study of lepton-pair production to below the ρ^0 and ω region ($m \lesssim 0.6$ GeV/c^2).[8-15] Less divergence exists among these studies than for the single-lepton experiments: All of the high-statistics experiments are consistent with an excess of lepton pairs over the sum of backgrounds and known particle decay sources. These pair yields are higher by an order of magnitude than are expected through the standard Drell-Yan model.

Study of the anomalous lepton pairs appears to be a more powerful way to explore possible dynamical sources than measurements of single-lepton yields. One avoids the dilution of information resulting from the parent-daughter relation between pair and single particle. Indeed, the pair experiments reported so far, including a short report on our own work,[14] have shown anomalous pairs to be mainly produced at low x and low p_T, and to be similar in dielectron and dimuon channels. In addition, pair experiments have typically used a large-solid-angle detection apparatus, which is rather well suited to exploration of the remaining particles in an interaction giving an anomalous pair.

A related subject to massive-e^+e^--pair production is the behavior of single-real-photon production. Clearly a natural extension of most electromagnetic mechanisms yielding e^+e^- will give a concomitant single-γ component. To date, the only positive reports[16] of inclusive γ production have been at large p_T and high s, where it is observed that γ/π is about equal to $x_T=p_T/p_T^{\max}$. Apart from reports[17,18] indicating the existence of very-low-energy bremsstrahlung photons, there are only upper limits on γ/π (Refs. 19 and 20) in 10—20-GeV πp collisions.

This paper presents the results of an experiment measuring inclusive e^+e^- production in π^-p collisions at 17 GeV/c. The large-solid-angle spectrometer was sensitive to e^+e^- pairs at Feynman x greater than 0.2 and masses up to about 1.5 GeV/c^2. In addition, we had good acceptance for charged particles and photons produced in these pair events and can thus perform a variety of searches for explicit decay contributions yielding anomalous pairs.

The organization of the paper is as follows. Section II describes the apparatus. Section III gives the experimental method and discusses the analysis method, determination of various backgrounds, and contributions to our pair sample from the main physical sources deriving from ρ^0, ω, and η decays. Results are presented in Sec. IV, both for the kinematic dependences of anomalous e^+e^- and for the structure and effective-mass combinations within the events containing the pair. Section V discusses these results, both in order to make connections and inferences on the related e/π and γ/π ratios and to confront the data with various proposed models for the source of anomalous leptons.

II. APPARATUS

The experiment was conducted at the multiparticle-spectrometer[21] (MPS) facility at Brookhaven National Laboratory. The MPS magnet provides an active volume of $1.8\times1.2\times4.6$ m^3 and was operated at a central field of 10 kG along the negative y axis. The coordinate system used has the z axis along the beam direction and y axis vertically upward.

A 17-GeV/c π^- beam was incident upon a 90-cm-long liquid hydrogen target located in the upstream end of the MPS field volume, as shown in the experimental arrangement of Fig. 1. Around the target there were 7 concentric cylindrical spark chambers (CSC's), and downstream of it 44 planar wire spark chambers (SC's), 12 planar proportional wire chambers (PWC's), and 2 transition-radiation detectors (TRD's), all within the field volume. Further downstream and outside of the magnet there

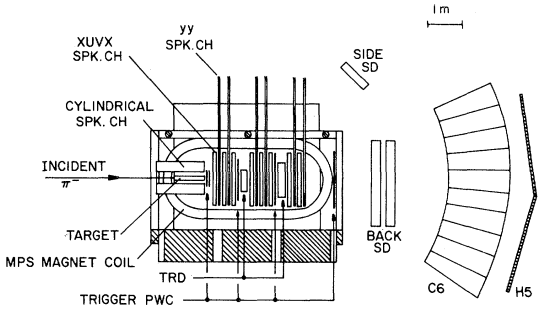

FIG. 1. Plan view of the experiment.

were two lead-scintillator shower detectors (SD's), four planar spark chambers, a scintillator hodoscope, and a freon Cherenkov detector. Electron-pair candidates were selected on-line by a fast electronic triggering system which demanded electron signals in the TRD's and SD's and a minimum hit multiplicity in the PWC's. The devices behind the SD's were used primarily in a charm-particle-search experiment, performed concurrently with this work.

The unseparated 17-GeV/c negative beam was operated with approximately 4×10^5 particles per 1.5-sec spill. The momentum acceptance was 1% [full width at half maximum (FWHM)]. A system of beam PWC's measured the incoming-particle momentum to $\pm0.1\%$. A Cherenkov counter in the beam tagged electrons; only nonelectron triggers were accepted.

The planar wire spark chambers were arranged in eight modules of x measuring chambers (horizontal coordinate) and six modules of y measuring chambers (vertical coordinate). The y modules each contained two measuring planes arranged (y,y) while the x modules contained four measuring planes arranged (x,u,v,x). The u and v coordinate axes were oriented $+15°$ and $-15°$ from the x axis to provide a means of associating x and y measurements.

All planes used a 9:1 neon-helium gas mixture with a trace of ethanol vapor and had a position resolution of 0.7 mm, adjacent spark resolution of 3 mm, and efficiency $\approx97\%$. A constant clearing field of 50 V/cm was maintained across each plane which gave a chamber memory time of 1 μsec. Just after triggering, the chambers were sparked with 5-kV pulses, and each gap was read out magnetostrictively from both ends along cathode wires. A 2-kV pulse was applied after sparking to clear away ions formed during the spark discharge.

The cylindrical chambers were composed of seven concentric gaps. Each gap was formed by an inner cylinder of wires oriented parallel to the z axis, and

an outer cylinder of wires wrapped helically about the z axis. The helical view had a pitch of $\pm 30°$ for the inner two gaps and $\pm 45°$ for the outer with signs alternating between adjacent gaps. Magnetostrictive readouts of both wire sets provided two position measurements of each spark with resolution of ± 1 mm (axial) and ± 1.4 mm (helical).

Five PWC's were used for triggering. Immediately downstream of the target was a single module containing x- and y-measuring PWC's called *TVX* and *TVY*. These two chambers had a circular active region of radius 25 cm. Further downstream, at approximately regular intervals, were three x-measuring PWC's of large rectangular aperture called *TPX*1, *TPX*2, and *TPX*3. Each trigger PWC was supplied with hardware logic to identify clusters (a series of consecutive wire hits) and provide a signal proportional to the number of clusters in the chamber as well as the rough cluster coordinate. The signals from the PWC cluster logic were used to impose charged-particle multiplicity requirements at the trigger level.

In addition to the trigger PWC's, seven more chambers of small aperture were used to provide in-time position measurements along the beam trajectory. These PWC's were very helpful in identifying out of time beam tracks appearing in the spark-chamber system.

All the PWC's described above were operated with a gas mixture of 80% argon, 15% isobutane, 4% dimethoxy methane, and 1% freon.

The two shower detectors provided electron and photon identification. They were constructed of alternating layers of lead radiator and acrylic scintillator sampling planes, and were optimized for maximum electron/hadron discrimination in the 2-to-10-GeV/c momentum range. A description of the shower detector and the details of the trigger electronics is given elsewhere.[22]

The two shower detectors were named for their positions relative to the MPS magnet: the back shower detector (BSD), and the side shower detector (SSD). The BSD was 18 sampling planes deep (z direction) and split into a top and bottom portion. The central 14 segments were 7.62 cm in width and the 5 outer segments on either side were 15.24 cm wide. The 18 sampling planes were combined into three layers (A,B,C) of six sampling planes each. The A, B, and C layers, containing 2.66, 3.51, and 5.21 radiation lengths, respectively, formed a module which sampled longitudinal shower development. One phototube for each layer viewed the six scintillator planes through a Plexiglas light pipe. In front of each segment was an additional scintillator (F for front layer) for distinguishing between photon and electron showers. The SSD was similarly constructed, but was 12 sampling planes deep (layers A,B), six segments wide and, because its photon acceptance was negligible, had no front counters. Its layers contained 3.51 and 5.21 radiation lengths, respectively. The analog shower-detector signals were both used in the trigger to identify electrons and photons as well as being recorded off-line for better particle identification. The trigger indicating an electron summed adjacent channels and for an electron candidate required 2.5 GeV in the BSD and 0.6 GeV in the SSD. It also required the pulse height of $A/(A+B+C)$ to be greater than 10% in the BSD. The position of the cells satisfying these conditions in the BSD were latched and recorded as well as serving as one coordinate for the RAM signal described below.

Each of the 216 SD phototubes was supplied high voltage through its own continuously adjustable divider circuit. Phototube gains were initially set by triggering on minimum-ionizing cosmic rays. The energy deposit from a minimum-ionizing particle was well below the amount required to trigger, so to calibrate at large energies, beam electrons from 4 to 15 GeV/c were steered into the BSD. Throughout the run, phototube gains were trimmed by comparing shower energies with the momenta of electron tracks reconstructed on-line. Gain variation was monitored frequently by flashing light-emitting diodes (LED's) fastened to the phototube light guides.

In order to reject hadron background at the level of 1 in 10^5, we installed transition-radiation detectors (TRD's) within the MPS field volume. Each TRD consisted of a stack of 750 Li foils (0.024 radiation lengths) in a He-filled box, and a PWC filled with 1.2 cm of 90% Xe–10% CO_2 at atmospheric pressure to detect x-ray photons. The signals on each wire measured ionization loss (dE/dx) in the Xe and transition radiation from the particles traversing the Li foil interfaces. The analog signal for each wire was amplified and split to an analog-to-digital converter (ADC) and to trigger electronics. Each overlapping set of three adjacent wires was summed and discriminators required a pulse height equivalent to 12 keV in photon energy deposited in a wire triplet to satisfy the electron trigger requirement. A typical hadron deposited 5 keV in ionization loss. Clusters were formed from adjacent hit triplets and the trigger logic then counted the number of TRD electron clusters. These cluster positions were also latched and recorded off-line as well as serving as the coordinate for the RAM signal as described below.

The TRD electronic gains were calibrated by using a capacitive strip across the PWC wires to deposit known quantities of charge on each wire, simu-

lating signals of 5- and 25-keV photons. Measurements of both low and high signals gave two constants for every channel; a slope in ADC counts per keV, and intercept in keV at 0 ADC counts. This two-parameter fit compensated for any nonlinearity of the ADC's for small signals. A more detailed discussion of the TRD system appears in Ref. 23.

The data for the experiment was collected using a variety of special trigger requirements. All electron triggers shared the basic trigger, ERAM:

$$\text{ERAM}=\text{B}\cdot\text{TP}\cdot\text{RAM}\ .$$

Here B denotes the coincidence of three beam scintillators and the beam PWC system indicating a single incident π^-, without a subsequent beam particle within 100 nsec. TP is the requirement on the trigger PWC multiplicities; it was set to require ≥ 2 hits in *TVX*, *TVY*, and *TPX*1 and ≥ 1 hit in the last two chambers, *TPX*2 and *TPX*3.

RAM denotes the correlation of hit positions in both TRD's and the BSD. A $128\times128\times128$-bit random-access memory (RAM) was addressed using the three separate electron devices to index each of the three coordinates.[24] The RAM was preprogrammed to set the bits at those nodes corresponding to valid combinations of hits resulting from the track of an e^- of $p\geq 2$ GeV/c. The RAM signal resulting from finding a valid spatial combination of TRD and BSD electron triggers thus indicated an electron track was present.

The trigger ERAM provided a minimum bias sample of inclusive electron production. Two additional triggers were used to give electron-pair events. The presence of an electron trigger for the SSD or an additional electron trigger in the left half of the BSD was taken as an indication of an e^+. The two triggers were

$$\text{PAIR A}=\text{ERAM}\cdot\text{BSD}\,e^+$$

$$\text{PAIR B}=\text{ERAM}\cdot\text{SSD}\,e^+\ .$$

PAIR A, with both e^+ and e^- demanded in the BSD, was sensitive primarily to pairs with Feynman $x>0.5$. PAIR B selected pairs down to $x=0.2$, with a peak in acceptance at about $x=0.45$.

All of the above triggers were prescaled in order to allow live time for the concurrent charm-production experiment. Other triggers were devised to obtain samples of γ conversions and K^0 and Λ decay. These were used primarily to study mass resolutions and to obtain samples of pure electrons or hadrons with which to measure electron/hadron discrimination.

III. ANALYSIS

The experiment collected above 6×10^5 events in the PAIR A and PAIR B triggers, in addition to the several special triggers used for calibration. The PAIR triggers were dominantly events with two electrons, but in addition to direct e^+e^- pair events there were photon conversions, electrons from two separate photon conversions, and some amount of hadron background. The main thrust of the event analysis then was the reconstruction of most of the tracks in each event in order to be able to identify the triggers due to events from these background processes.

Calibrations for the experiment were updated for each of the approximately 700 data tapes. These included the parameters associated with the $\vec{E}\times\vec{B}$ drift of ions in the spark chamber, gain constants for conversion of SD and TRD signals to energy, and spark-chamber fiducial constants.

Each event was subjected to tests before attempting its reconstruction. The beam track measured by the beam PWC's was required to be unambiguous and seen in each chamber. The recorded number of clusters in the five trigger PWC's within the MPS were required to satisfy the trigger multiplicity condition. Both TRD's and SD's were required to have the appropriate number of electronlike signals.

The central problem of event reconstruction was that of recognition of tracks from the array of sparks presented by the various chambers. It was particularly important that a low momentum, short track be found efficiently in order to guard against an asymmetric e^+e^- pair masquerading as a single electron. The search for possible pairings of all observed electrons was a recurrent theme, mounted with increasing sophistication as the analysis progressed. The initial pattern recognition algorithm searched in all the planar spark chambers and PWC's for track segments in both $x-z$ and $y-z$ projections and then linked segments using the u and v coordinate hits. Any event which did not yield two tracks was abandoned. Any event which left more than 40% of its recorded hits unassigned to tracks was also discarded. Each recognized track was characterized by the fraction of PWC's which were traversed and showed a hit. A low fraction signified that the track was likely to be accidental (out of time with the trigger). In this way most of the out of time tracks were eliminated.

The second main task for event reconstruction was the identification of electrons. In the case of the TRD's, we had information from the TRD-PWC on the location of an energy deposit above 12 keV from discriminators that formed the trigger and were recorded in latches. An electron candidate

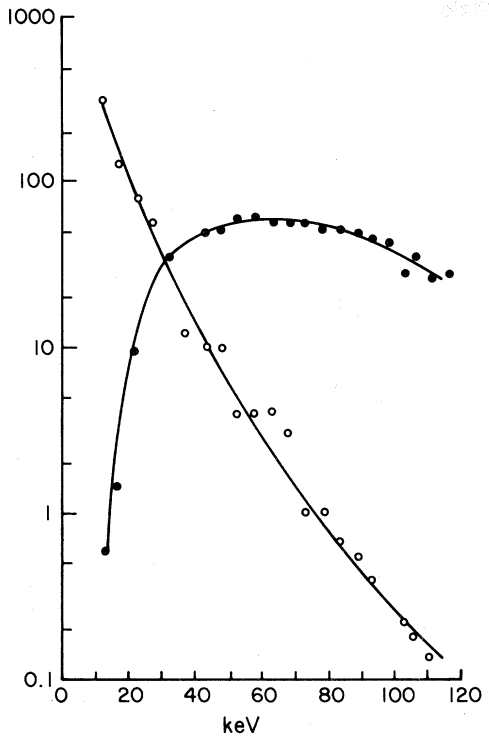

FIG. 2. Number of events versus energy deposit in a TRD for samples of electrons (closed circles) and pions (open circles).

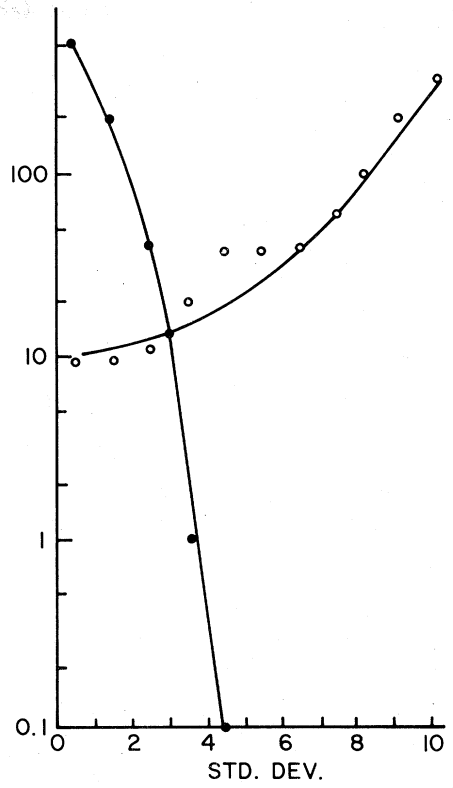

FIG. 3. Number of events versus standard deviations, $|E/p-1|/\sigma$ for the back shower detector. E is the energy deposited, p is the momentum measured in the MPS, and σ is the standard deviation.

track was required to be correlated with such a hit. The signal charge for each TRD-PWC wire was recorded; in the analysis, we formed clusters of energy deposit in both TRD's. The distribution in energy for pure electron and hadron samples is shown in Fig. 2. The pure electron sample is taken from tracks which (a) can be constrained to a γ conversion and (b) are identified as electrons in the SD and other TRD. The pure hadron (pion) sample is neutral vee decay prongs consistent with $K^0\to\pi^+\pi^-$ (taken with special triggers). The track of each electron candidate was also required to be consistent with such an energy cluster.

An electron track candidate was also required to agree with the appropriate SD hardware latch indicating a large energy deposit. In addition, the signal charge of each layer of each SD cell was recorded, so that clusters of energy could be found in later analysis. We demanded that an electron track candidate extrapolate to such a cluster. To identify an electron we compared the energy (E) measurement from the SD to momentum (p) from magnetic measurement. We define $|E/p-1|=\eta$; Fig. 3 shows the distribution of events in η/σ_η for both pure electron and hadron samples in the BSD.

Rather than employ cuts on TRD energy deposit distributions and SD η distributions separately, we preferred to form a single quantity from all available information. For a particular track in a TRD, the relative probability for the particle to be an electron or hadron could be assessed from the curves in Fig. 2. Similarly, the relative probability for electron or hadron in the SD can be obtained using Fig. 3. We define these relative probabilities to be

$$r_j=P_e^{(j)}/P_{\text{had}}^{(j)}$$

for any device, j, through which the track passes (and set $r_j=1$ if the track misses the device). The measure of the likelihood for the track to be an electron is then the product of the r_j's for each individual device. Figure 4 shows the r distribution for pure electrons and pure hadrons in a TRD. Figure 5 shows the r distribution of BSD and SSD. The trigger e^- must traverse both TRD's and the BSD; the same is true for almost all PAIR A e^+. The

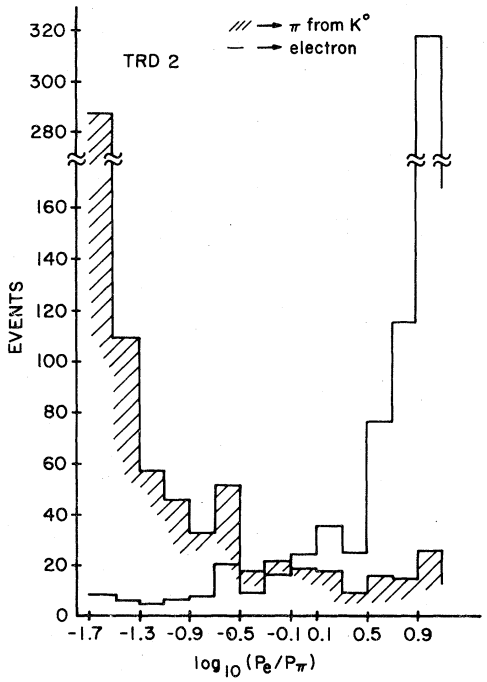

FIG. 4. Number of events vs $\log_{10}(P_e/P_\pi)$ in a TRD for samples of electrons and pions. P_e and P_π are the relative probabilities for the deposited energy to conform to electron or pion energy-deposit distributions.

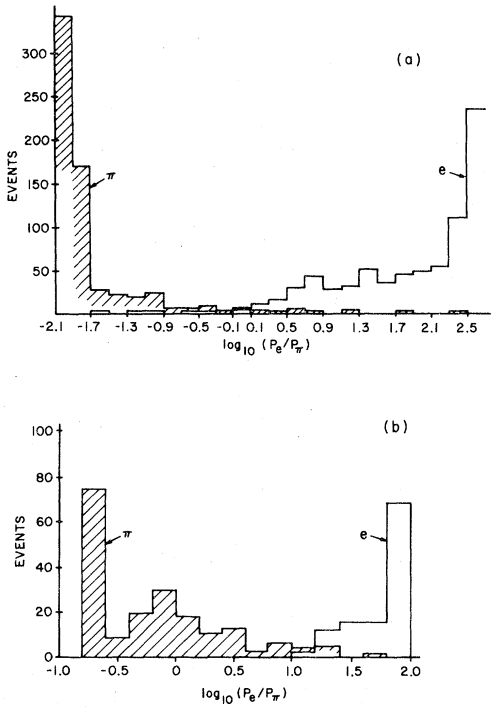

FIG. 5. Number of events vs $\log_{10}(P_e/P_\pi)$ in (a) back shower detector and (b) side shower detector for samples of electrons and pions. P_e and P_π are the relative probabilities for $(E/p-1)/\sigma$ to conform to the distributions for electrons or pions.

PAIR B e^+ is seen in the SSD only. The product of the r values for the three device hits is required to exceed 1000; this cut retains 80% of all electrons and rejects in excess of 99.9% of the hadrons. The PAIR B e^+ is selected by $r_{\rm SSD} \geq 32$; this leads to a 99% rejection of hadrons. (Determination of the hadron rejection factors was limited by the size of the pure hadron sample.)

Those tracks which were identified as electrons by the combined TRD and SD information were called trigger electrons. We have demanded that the trigger electron tracks have a hit in the first PWC planes downstream of the target to eliminate photon conversions outside of the hydrogen target. Events were required to have at least two trigger electrons.

Each trigger electron was then subjected to a test, called $e\bar{\gamma}$, to see if it could have been a member of a photon conversion (internal or external) in which the other pair member was not a trigger electron. Each trigger electron was taken together with all nontrigger tracks of the opposite sign to compute the invariant mass of the putative e^+e^- combination. If the mass was less than 100 MeV/c^2 and the distance of closest approach was less than 1.5 cm, the trigger electron was removed from the sample. This $e\bar{\gamma}$ requirement was refined and reapplied later in the analysis as the track determination was refined. The tracks of all surviving events were now subjected to kinematic fitting in the actual magnetic field of the MPS. The tracks from cylindrical spark chambers were also fit. An effort was made to refine the pattern-recognition spark lists by omitting hits not in agreement with the fit, adding new hits, and joining segments of a common trajectory. A one-constraint (1C) fit to all oppositely charged track pairs was made to K_s^0, Λ, and $\gamma \to e^+e^-$ hypothesis. A list of all such neutrals which had a reasonable fit was prepared. At this stage, all trigger electrons remaining outside the conversion pair list were again subjected to the $e\bar{\gamma}$ test, this time using a 1C fit to the $\gamma \to e^+e^-$ hypothesis. Finally, the list of energy clusters in the BSD was searched for photon candidates. A photon was defined as a cluster unassociated with any track, with energy spread over at least two of the three layers in depth and exceeding 200 MeV. Clusters which were split between top and bottom halves of the BSD were merged into a single photon. The hit coordinate in x for a γ at the BSD was measured to within ± 3 cm; the y coordinate was

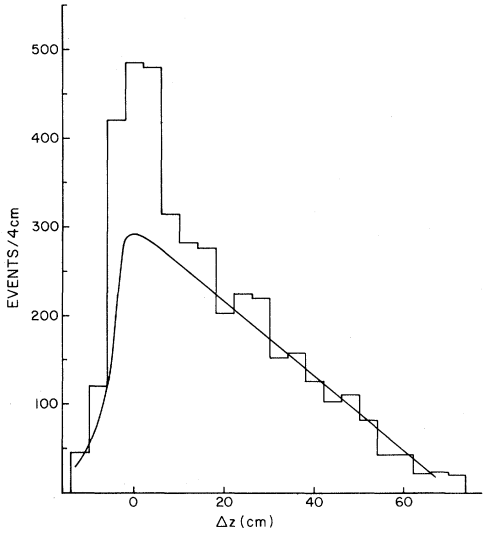

FIG. 6. Number of weighted events versus the separation Δz between production vertex and fitted conversion point. The curve shows a fit to the subset of external conversions. The weighting procedure is discussed in the text.

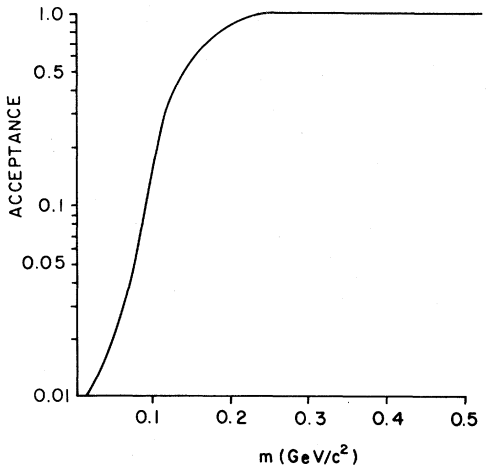

FIG. 7. Acceptance for direct e^+e^- pairs versus pair mass. The drop at low mass is due to the loss of events in analysis from removal of pairs which fit an external conversion hypothesis.

poorly measured in our detector (except when the cluster was split between top and bottom) and was assigned the most likely y position from a Monte Carlo simulation of inclusive photon production.

The complete list of both charged and neutral tracks assembled was now subjected to a topological analysis to establish the production vertex and decay or conversion vertices. This iterative analysis tried many combinations of particles participating in the primary vertex. In particular, a trigger electron pair was subjected to a constrained fit for a $\gamma \rightarrow e^+e^-$. If successful, these electrons were tried both as a direct (internal conversion) pair and external conversion pair. Events for which no acceptable χ^2 was found or the trigger electrons could not be satisfactorily included in primary or secondary vertices were discarded.

The remaining events were classified as follows.

Conversion. The γ hypothesis was accepted and external conversion was favored.

Direct. The direct production of a pair was favored over external conversion, even if the pair could be constrained to a γ.

High mass. The subset of direct pairs in which the γ hypothesis was untenable.

Those PAIR A events for which the γ hypothesis is satisfied are plotted in Fig. 6. The abscissa is the difference in z between conversion point and primary vertex. Each event is weighted by the inverse of the conversion probability (based on the available length liquid H_2 available to the photon). The excess at $\Delta z=0$ is to be interpreted as being due to Dalitz decay of π^0 (and η,ω). The ratio of Dalitz decay events to external conversions ($\Delta z>0$) allows us to deduce the π^0 Dalitz decay branching ratio in good agreement with its measured value. Figure 6 also shows that the γ conversion point is measured to within ± 10 cm; the external conversions with $\Delta z > 20$ cm do not contaminate our direct sample of pairs.

The acceptance for e^+e^- pairs in this experiment has been studied with the aid of Monte Carlo simulation. The variables pertinent for this calculation are pair mass m, Feynman x, transverse momentum p_T, and the decay angle θ (of the e^+ relative to the pair momentum in the pair rest frame). The mass acceptance of the apparatus has been determined to be essentially uniform for $m \leq 0.8$ GeV/c^2 and gently falls off above this value. There is, however, a low-mass cutoff imposed in the analysis due to the exclusion from the high-mass category of pairs satisfying the γ constraint. Monte Carlo events have been generated to study this effect; the resulting cutoff in mass acceptance for high-mass events is shown in Fig. 7. We have studied the acceptance in x and p_T by generating a uniform distribution of events in x and p_T for fixed m and a specific distribution in $\cos^2\theta$. The resulting fraction of accepted events in each (x,p_T) interval gives the acceptance. The acceptance in (x,p_T) was shown to be insensitive to the value of m and was also similar to that

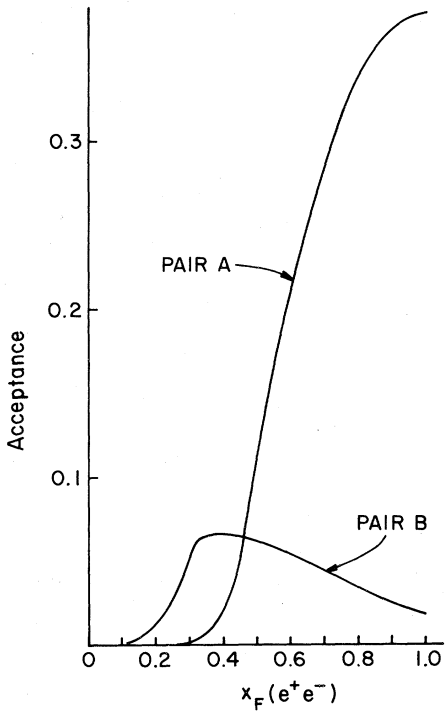

FIG. 8. Acceptance for direct e^+e^- pairs versus x for both triggers used in this experiment. Acceptance here is integrated over the p_T and mass distribution expected for high-mass pairs from $\eta \to \gamma e^+e^-$.

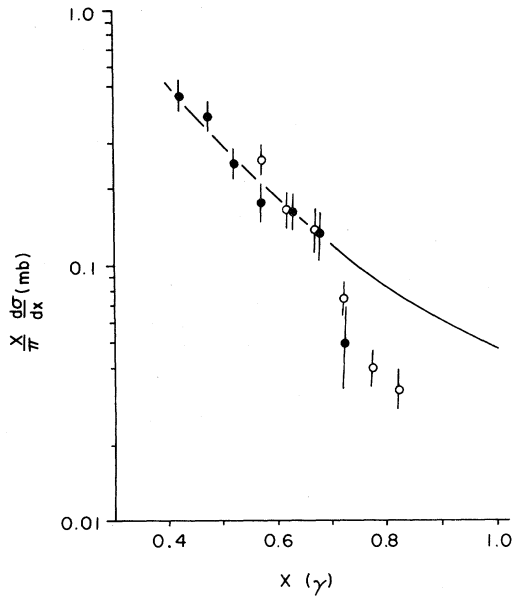

FIG. 9. Measured invariant cross section for inclusive γ production versus x. Open circles are for PAIR A triggers and closed circles are for PAIR B. The solid line represents the data of Ref. 25.

obtained using pairs resulting from Dalitz decay of π^0 using known π^0 production cross sections. The acceptance for PAIR A and PAIR B as a function of x, integrated over p_T are shown in Fig. 8. The p_T dependence is negligible at large x; for $x<0.5$ the acceptance falls approximately linearly with p_T.

There is an effect on acceptance due to the $\cos^2\theta$ distribution chosen. We have used a flat $\cos^2\theta$ distribution for our high-mass acceptance; assumption of a $\sin^2\theta$ or a $(1+\cos^2\theta)$ distribution would change the acceptance by about $\pm 30\%$. This ambiguity is not present for the low-mass Dalitz sample of events, as the $\cos^2\theta$ distribution in this case is known.

The direct pair events obtained from Fig. 6 (and the similar plot for PAIR B), after subtracting the effect of close external conversions, have been used to compute the inclusive photon production cross section. Figure 9 shows the invariant cross section as a function of x for our data as compared with that obtained from an 18-GeV $\pi^- p$ experiment in a hydrogen bubble chamber.[25] Below $x=0.7$ the agreement is good, thus verifying the absolute normalization of our data. Above $x=0.7$, our experiment for low-mass pairs suffers from a trigger bias due to our requirement of at least two hits in the most upstream y-measuring PWC. At large x, the associated-charged-particle multiplicity is low, and the low-mass-pair electrons themselves merge their hits in this PWC yielding just one hit.

The distribution of events from the high-mass sample with pair mass is shown in Fig. 10 for both PAIR A and PAIR B triggers. Both samples display a rapidly falling distribution with mass in the region $0.2 \le m_{ee} < m_\rho$. The PAIR A sample shows a clear signal due to the production of ρ^0,ω, with subsequent direct decay into e^+e^-.[26] The direct decays of ρ^0 and ω afford another check of the absolute normalization of the experiment. Using the known inclusive ρ^0 and ω production cross sections,[27] our acceptance, efficiency, and known branching ratio,[28] we predict 60 ± 10 ρ,ω direct decays in our PAIR A sample to be compared with the 54 ± 8 observed. For PAIR B we predict 10 ± 2 events, consistent with what is observed.

There are several known internal-conversion decays which contribute to the continuum region $m < m_\rho$: they are $\pi^0 \to \gamma e^+e^-$, $\eta \to \gamma e^+e^-$, and $\omega \to \pi^0 e^+e^-$. Our mass cutoff in analysis for full acceptance of 0.2 GeV/c^2 eliminates π^0 sources of electron pairs. In order to establish the existence of an anomalous direct electron-pair signal, we thus

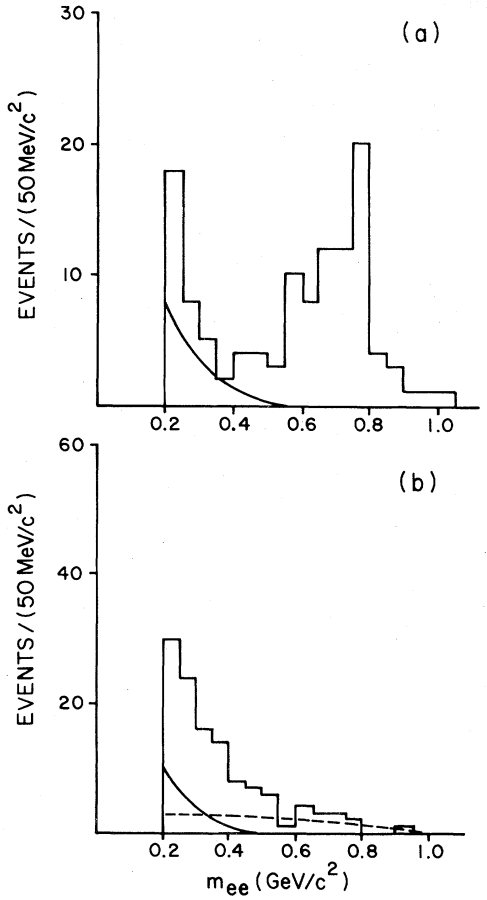

FIG. 10. Mass spectrum for electron pairs from (a) PAIR A and (b) PAIR B. The solid curve is the background computed for η and ω internal conversions (see text). The dashed curve is the background due to hadron misidentification.

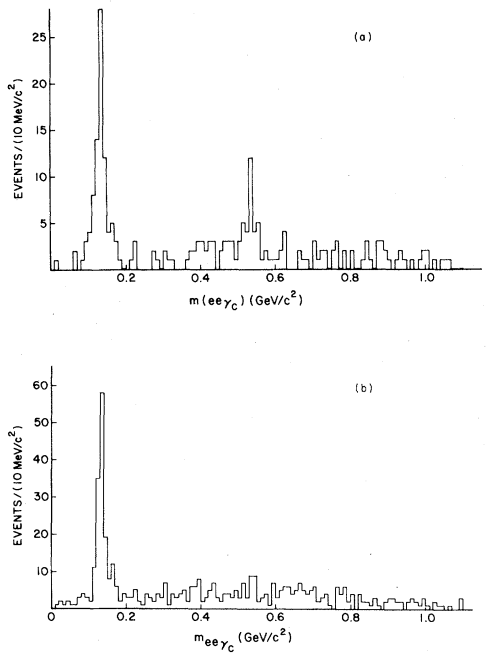

FIG. 11. Effective-mass distribution for $e^+e^-\gamma$ for (a) PAIR A and (b) PAIR B. The γ is from conversions within the MPS.

focus on the η and ω decays in the interval $0.2 \leq m \leq 0.6$ GeV/c^2.

The contribution of η and ω internal-conversion decays to our mass spectra has been computed in two independent ways. The first method used the previously measured η/ρ and ω/ρ ratios[29] and our direct $\rho,\omega \to e^+e^-$ signal. Inclusive production of η,ω,ρ are measured to occur in the ratio 0.34:0.9:1 in 16-GeV/c $\pi^- p$ collisions and show similar distributions in x and p_T. Using known mass distributions and branching ratios[28,30] and our Monte Carlo acceptances as a function of x and p_T for each particle production decay, we have determined the ratio of electron pairs from $\eta \to \gamma e^+e^-$ or $\omega \to \pi^0 e^+e^-$ in each mass interval to the electron pairs from direct decay of ρ^0 and ω. The mass distribution of electron pairs from internal conversion decays computed in this way is also shown in Fig. 10. For the PAIR A sample, the observed number of direct ρ^0,ω decays is 54 ± 8; the number of internal conversion pairs for $0.2 \leq m \leq 0.6$ GeV/c^2 is 22 ± 8. In the case of the lower-x PAIR B trigger events, the number of ρ^0,ω direct decays is much smaller and cannot be determined in our data. We have used our observed PAIR A sample of ρ,ω decays and the known production cross section[27] and acceptance variations with x to predict 10 ± 2 events from direct ρ,ω decays in the PAIR B sample. The resulting number of internal conversion pairs for $0.2 \leq m \leq 0.6$ GeV/c^2 is 22 ± 8 events. The η decays dominate over ω decay by a factor of 2.1 and 1.8 for PAIR A and PAIR B samples, respectively.

An independent determination of the η internal conversion background can be made from our data using the reconstructed decays $\eta \to \gamma e^+e^-$, where the γ converts within the fiducial volume of the MPS and the conversion electrons are fitted. Figure 11 shows these events for both trigger types and low-mass pairs; for PAIR A both π^0 and η signals are clearly seen, while for PAIR B the η is negligible. For the raw sample of observed γe^+e^- events, the η/π^0 ratio is 0.27 ± 0.10 for PAIR A and 0.00 ± 0.07 for

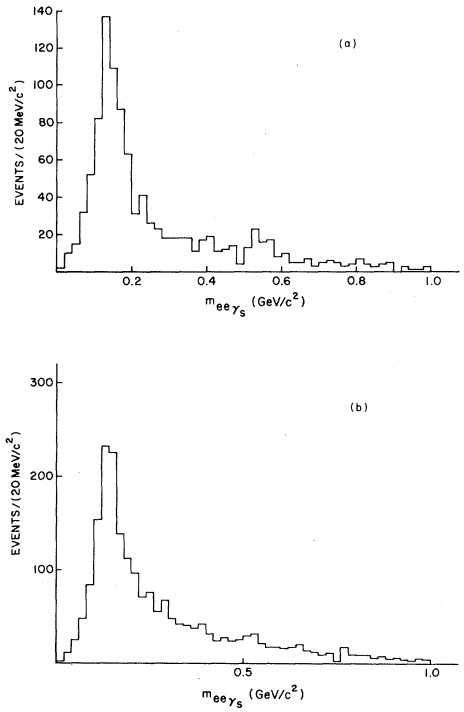

FIG. 12. Effective-mass distributions for $e^+e^-\gamma$ for (a) PAIR A and (b) PAIR B. The γ is from shared showers in both top and bottom halves of the BSD.

PAIR B. The number of π^0 internal conversions in our samples is known from Fig. 6 after correction for the low-mass pairs from close conversions. Further correction for the relevant branching ratios, cross-section dependences on x and p_T, and acceptances yield total numbers of η internal conversions to be 124 ± 46 for PAIR A and less than 314 (2σ limit) for PAIR B. The accompanying contribution from $\omega\to\pi^0e^+e^-$ is established using the published η/ω ratios.[29] The final contribution from both sources for $m\geq0.2$ GeV/c^2 is 9.6 ± 3.6 (PAIR A) and <26.2 (at the 2σ level for PAIR B).

The result above, based on reconstruction of γ conversions in the MPS, suffers from low statistics due to the low conversion probability within the chamber system. Virtually all γ's are detected in the BSD; however the lack of a y-coordinate determination for these showers precludes adequate mass resolution, except in the special case that the shower is shared in the upper and lower halves of the detector. The γe^+e^- mass distribution for this category of events is shown in Fig. 12, where the η signal may be just discernible. The limits on the internal-conversion background pairs to our high-mass sample from these events agree well with those from the conversion γ sample.

In subsequent analysis, we have used the background calculation for η and ω decays from the first method (based on the previously measured $\eta{:}\omega{:}\rho$ ratios), although it is larger than our own direct determinations. We feel that it is likely in fact that inclusive η production may be smaller than that inferred in Ref. 27 in which the measured quantity was the ratio of $\eta{:}\rho^0$ in events containing no additional neutral final-state particles.

There are two sources of events to the distributions of Fig. 10 from misidentifications in the final state. The first of these is due to hadrons, misidentified as electrons. The second is due to real electron pairs in which the e^+ and e^- originate from different γ's.

The hadron background contribution was determined using the basic ERAM trigger which selected an unbiased sample of inclusive e^- events. Since our analysis rejected all candidate high-mass electron pairs if either member could be included in a low-mass pair fit with any other track, the hadron misidentification background can occur only when the other member of an e^+e^- pair escapes our detection ($p\lesssim0.1$ GeV/c). We have selected those events from the ERAM trigger in which no evidence of the e^+ partner is seen. In this sample, we analyze all pairings of e^--hadron$^+$ in which the hadron enters the BSD or SSD, taking the hadron to be an e^+ for this analysis. Using the known hadron rejection probabilities for BSD and SSD we can compute the expected number of eh pairs in our final PAIR A and PAIR B samples. For PAIR A, we find $3.0\pm0.5e^-h^+$ and e^+h^- events. In the PAIR B sample we obtain 32 ± 6 events (all e^-h^+), distributed smoothly in mass out to $m\simeq1$ GeV/c^2. These background events are indicated in Fig. 10(b).

The e^+e^- events from separate γ conversion are also determined from the unbiased ERAM e^- sample. An event enters this category only when both companion electrons from the two low-mass pairs escape detection. We again select the ERAM events in which only a single e^- is observed. The γ's observed in the BSD for these events are then collected and used in a Monte Carlo calculation to compute the probability for a second conversion to occur, with a detected e^+ and unseen e^-. The fictitious events, with the second conversion included, are then subjected to all analysis vertex requirements. We conclude 0.5 ± 0.3 events from two conversions are included in our PAIR A sample (for $0.2\leq m\leq0.6$ GeV/c^2) and 2.5 ± 1.0 events in the same mass interval for the PAIR B sample.

TABLE I. Events for $0.2 \leq m \leq 0.6$ GeV/c^2 ($m = e^+e^-$ pair mass).

	PAIR A	PAIR B
Total	59 ±7	106 ±10
η,ω internal conversion	22 ±8	22 ± 8
Hadron background	1.4±0.3	19 ± 5
Two-photon background	0.5±0.3	2.5± 1.0

IV. RESULTS

The event distributions shown in Fig. 10 are summarized in Table I, with the number of events due to backgrounds and internal conversions indicated for both triggers in the mass interval $0.2 \leq m \leq 0.6$ GeV/c^2. The residual events not attributable to a known source are called the anomaly. For PAIR A, the anomaly is small, while for PAIR B it is large and significant. The mass distributions of anomalous events, for both triggers are shown in Fig. 13.

It is apparent that anomalous e^+e^- pairs are more copious at low mass. Curves corresponding to m^{-1} and m^{-2} are shown for the PAIR B data in Fig. 13(b). An inverse square mass distribution seems favored, but owing to our uncertainties on the low-mass acceptance and background subtraction, we cannot rule out m^{-1} or m^{-3} shapes.

The distribution of direct e^+e^- pair cross section in x is shown in Fig. 14, after combining our two trigger samples. The anomaly is a strikingly central (low-x) phenomenon, as foreshadowed by the size of the effect in PAIR B relative to PAIR A. The background from η and ω decay is less central. Our data for anomalous pairs is well represented by the simple parametrization

$$\frac{d\sigma}{dx} = (3.9 \pm 1.4\ \mu\text{b}) e^{-(5.5)\pm(0.7)x},$$

for all p_T and $0.2 \leq m \leq 0.6$ GeV/c^2.

The event distribution in p_T^2, for events with $x < 0.5$, and $0.2 \leq m \leq 0.6$ GeV/c^2 is shown in Fig. 15. The data is adequately parametrized by a form

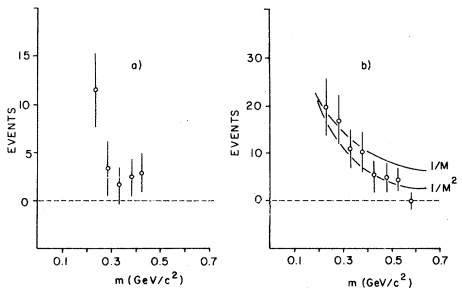

FIG. 13. Mass spectrum for electron pairs from (a) PAIR A and (b) PAIR B after subtraction of η and ω internal conversion pairs and backgrounds.

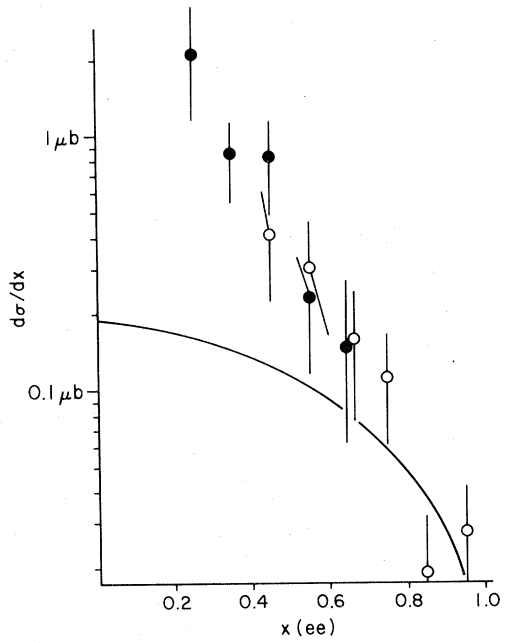

FIG. 14. Cross section for inclusive electron pair production versus x for the pair. Open circles are data for the PAIR A trigger; solid circles are for PAIR B. The solid curve is the expected contribution to these data from internal conversions of η and ω.

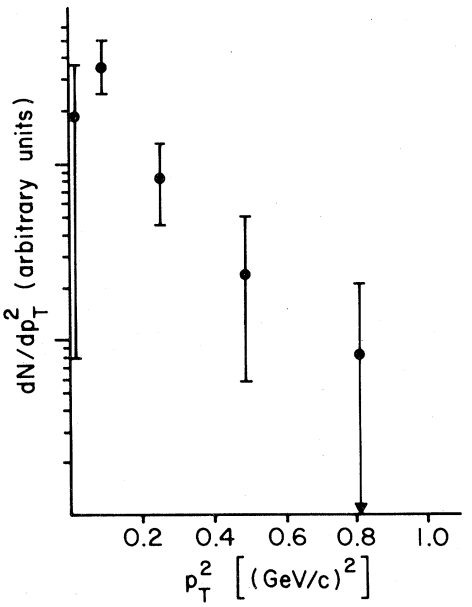

FIG. 15. Distribution of events with p_T^2 for electron pairs in the interval $x \leq 0.5$ and $0.2 \leq m \leq 0.6$ GeV/c^2.

TABLE II. Low-mass-pair experiments.

Experiment	Beam	Target	Momentum	e^+e^-	x interval
This exp.	π^-	p	17 GeV/c	e^+e^-	0.2–1.0
Ref. 13	π^-	p	16	e^+e^-	0.1–0.45
Ref. 10	π^+,π^-	p	15.5	$\mu^+\mu^-$	0.4–1.0
Ref. 11	π^+,π^-	p	18	e^+e^-	(−0.25)–0.25
Ref. 15	p	Be	13	e^+e^-	$\simeq 0$
Ref. 8	p,π^+	Be	150	$\mu^+\mu^-$	>0.15
Ref. 9	p	W,Fe,C	28	$\mu^+\mu^-$	0.3–0.7
Ref. 32	p	Cu	400	$\mu^+\mu^-$	0.15–0.5

$d\sigma/dp_T{}^2 \propto \exp(-Bp_T{}^2)$ with $B \simeq 6$ $(\mathrm{GeV}/c)^{-2}$. However, we note a correlation between the p_T distribution and the x value as discussed below.

There have been various other experiments sensitive to the production of low-mass dilepton anomalies. Lepton type, x interval, beam and target particles, and energy vary from one experiment to another. Table II shows the conditions for these experiments. All of the experiments with adequate statistics agree that there is a low-mass component of the lepton-pair spectrum which cannot be accounted for by known meson decay sources. They also agree that the low-mass anomaly is strongest at small x.

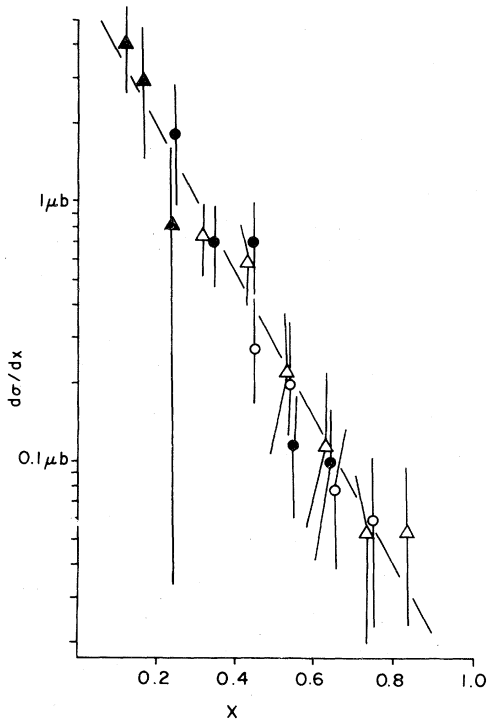

FIG. 16. Anomalous-lepton-pair inclusive cross section versus x of the pair. Circles are electron pairs from this experiment (closed circles for PAIR A and open for PAIR B); closed triangles are electron pairs from Ref. 13, and open triangles are muon pairs from Ref. 10. Electron pairs are weighted as dimuons as discussed in the text.

Comparison of dimuon and dielectron data can be facilitated if we assume that the lepton mass enters the production cross sections through the factor

$$f(z)=(1+2z^2)(1-4z^2)^{1/2},$$

where $z=m_e/m$. This function is what is expected if dileptons are produced by virtual photons. With electron pairs converted to pseudodimuons in this way, the x distributions of our experiment, the 16-GeV electron pairs,[12,13] and the 16-GeV muon pairs[10] agree well, as shown in Fig. 16. The combined data can be fitted by

$$\frac{d\sigma^{(\mu\mu)}}{dx}=(5.5\pm 2.1\ \mu\mathrm{b})e^{-(6.0\pm 0.9)x}$$

after known backgrounds are subtracted.

The 225-GeV data for $\pi^+p\to\mu^+\mu^-$ (Ref. 8) has been analyzed in Ref. 13 and a background subtraction was performed. It was found that anomalous pairs dominate over the known sources for $x \lesssim 0.3$. After background subtraction, the cross section can be fitted to an exponential x distribution with a slope of 15.9. Thus there is clear indication that the anomalous pair cross sections in πN collisions do not scale with energy. This conclusion is at odds with the situation reported for $\mu^+\mu^-$ production in pp collisions at 28 (Ref. 31), 150 (Ref. 8), and 400 GeV (Ref. 32). A comparison of these data[9] has found a similar exponential slope of around 10. However, these data at relatively large x contain a small fraction of anomalous dimuons and extracting the scaling behavior for the anomaly is difficult.

The p_T dependence of anomalous pairs can also be compared for the several dilepton experiments. Figure 17 shows the distribution in $p_T{}^2$ for our experiment and the other dielectron experiment.[12,13] Within errors, the distributions are the same; howev-

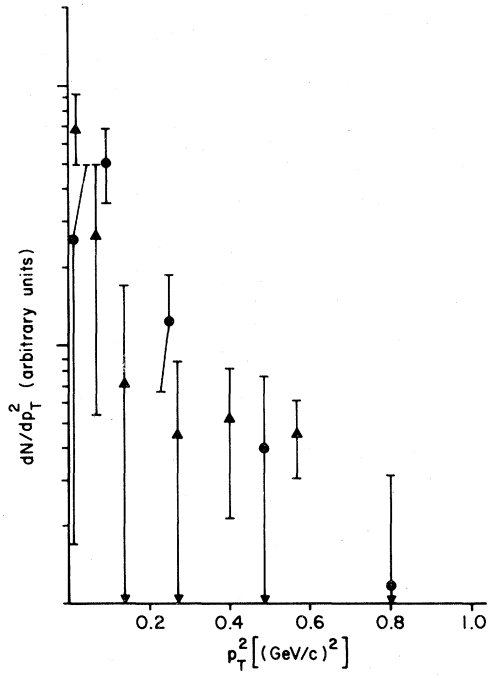

FIG. 17. Distribution of events p_T^2 for anomalous electron pairs. Circles are data from this experiment; triangles are data from Ref. 13.

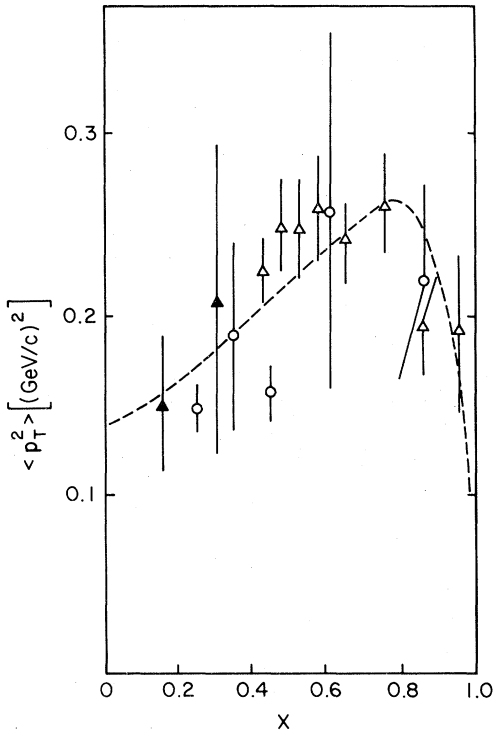

FIG. 18. Mean p_T^2 versus x for anomalous lepton pairs versus x. Open circles are electron pairs from this experiment, closed triangles are electron pairs from Ref. 13, and open triangles are muon pairs from Ref. 10. Electron pairs are weighted as dimuons as discussed in the text.

er the x acceptance of the two samples are different. It thus is interesting to examine the mean p_T^2 in different x intervals for anomalous pairs. Figure 18 shows this dependence for the three low-energy experiments (with dileptons weighted as dimuons); the dashed line shows the prediction for $\langle p_T^2 \rangle$ for the pairs originating from η,ω internal conversions. The anomaly clearly resembles these known sources in the p_T distribution, although it is significantly different in the x distribution as discussed above. The higher-energy result[8] also shows a strong similarity between $\langle p_T^2 \rangle$ for anomaly and pairs from η and ω decays.

Since this experiment had good detection efficiency for both charged particles and photons above 0.2 GeV, we have examined many properties of events containing anomalous electron pairs to probe for possible mechanisms of their production. The anomalous pair event sample for these studies is defined as those events containing a pair with $0.1 \leq m \leq 0.6$ GeV/c^2 and $x < 0.5$. In studying properties of anomalous events, we use comparison samples taken from low-mass events ($m < 0.1$ GeV/c^2) and $x < 0.5$. We also define a background sample in which the e^+e^- pair in the event has been substituted for by a random pair from another event.

We have constructed effective-mass distributions for a variety of final states involving e^+e^-, $\pi^\pm$, π^0, and γ. Here, charged tracks not identified as electrons are taken as $\pi^\pm$. π^0's are taken from acceptable 1C fits to $\gamma\gamma$ or $e^+e^-\gamma$ combinations in the low-mass sample and only $\gamma\gamma$ combinations in the anomalous events.

To illustrate the fitting procedure involving 1C-fit π^0's, we show $\pi^0\pi^-$, $\pi^0\pi^+$, and $\pi^0\pi^+\pi^-$ mass combinations in Figs. 19 and 20, where the π^0 is constrained from $e^+e^-\gamma$ from the low-mass sample. These pairs are thus dominated by π^0 Dalitz decay. We see clear ρ^- and little ρ^+ production, as expected with an incident π^- beam. In the $\pi^0\pi^+\pi^-$ combination, a small very narrow ω peak is also observed. The ω is contained in one 50-MeV bin. The resolution attained in the MPS is demonstrated by Figs. 21 and 22, where we observe the effective masses of $\pi^0(e^+e^-\gamma)$ and $K_S(\pi^+\pi^-)$. Their FWHM are, respectively, 20 and 15 MeV. The narrowness of these three- and two-particle effective mass combinations demonstrates that we are capable

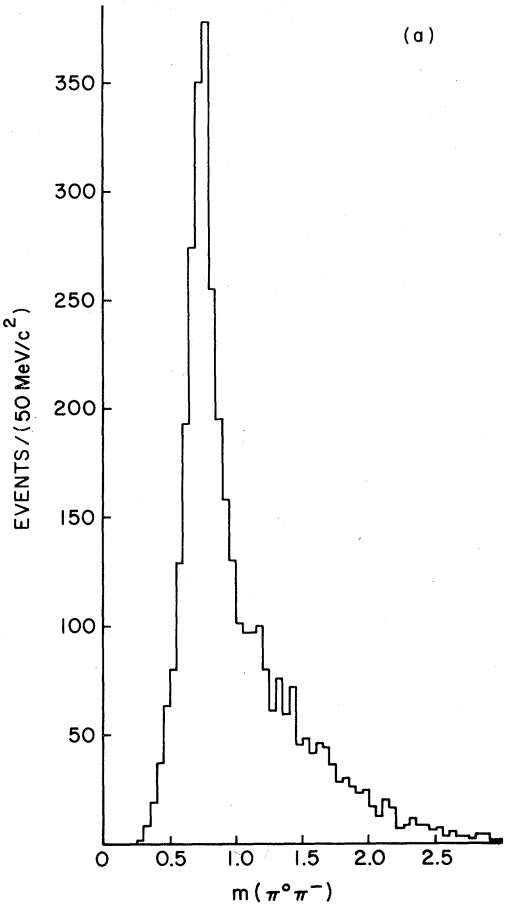

FIG. 19. Effective-mass distributions of dipions taken from low-mass direct sample of events for (a) $\pi^0\pi^-$ and (b) $\pi^0\pi^+$. The π^0 is a constrained fit from $e^{\mp}e^-\gamma$ combinations.

of seeing any narrow structure if it exists.

The fact that the mass and p_T dependence of the anomaly is very much like that of the η-Dalitz-decay e^+e^- pairs suggests a search for a possible

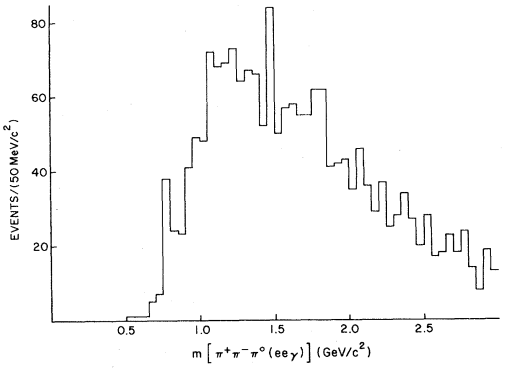

FIG. 20. Effective-mass distribution for $\pi^+\pi^-\pi^0$ combinations from the low-mass direct sample of events. The π^0 is a constrained fit from $e^+e^-\gamma$ combinations.

pseudoscalar state X, where $X\rightarrow e^+e^-\gamma$. Figure 23(a) shows the high-mass $e^+e^-\gamma$ mass spectrum and Fig. 23(b) the background distribution using e^+e^- pairs and photons from different events. Our expected $e^+e^-\gamma$ mass resolution of 120 MeV FWHM for the η, normalized to the expected sample of 20 events, is also shown in Fig. 23(a).

The $e^+e^-\pi$ effective mass combinations are shown in Fig. 24 for all three charges. In each case, the distributions are indistinguishable from the corresponding background samples obtained by substi-

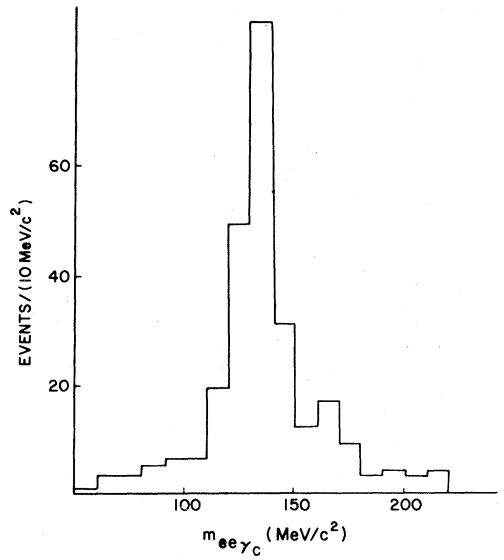

FIG. 21. Effective-mass distributions for $e^+e^-\gamma$ combinations taken from the low-mass direct sample of events. The γ is observed as a conversion in the MPS.

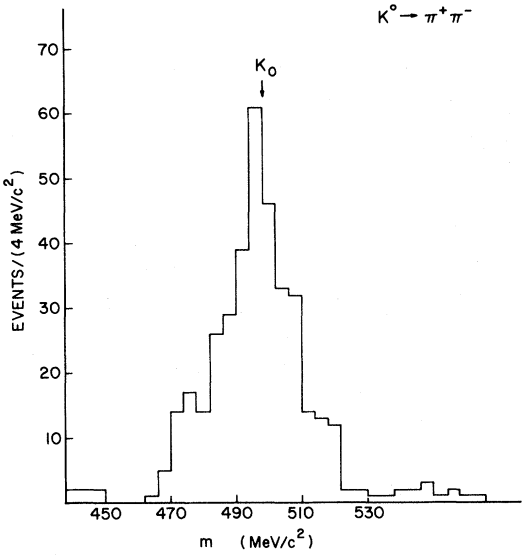

FIG. 22. Effective-mass distribution for $\pi^+\pi^-$ combinations taken from a special neutral-vee trigger.

tution of random e^+e^- pairs. Following a suggestion[33] that the internal conversion component of radiative decays of spin-2 mesons could contribute appreciable low-mass pairs, we have searched possible

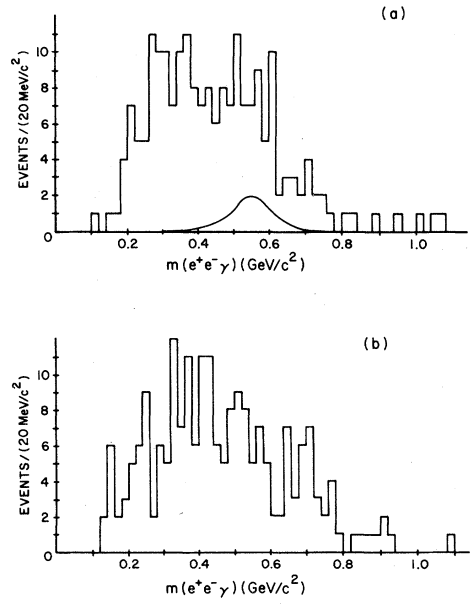

FIG. 23. (a) Effective-mass distribution for $e^+e^-\gamma$ combinations taken from the anomalous-pair sample of events. The solid curve shows the expected contribution from $\eta\rightarrow e^+e^-\gamma$. (b) Background $e^+e^-\gamma$ combinations obtained from random combinations of e^+e^- and γ from our anomalous-pair sample.

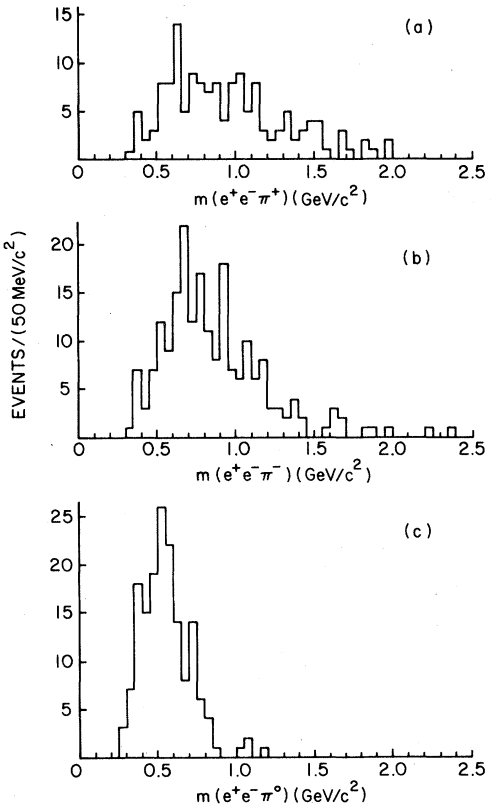

FIG. 24. Effective-mass distributions for (a) $e^+e^-\pi^+$, (b) $e^+e^-\pi^-$, and (c) $e^+e^-\pi^0$ combinations taken from the anomalous-pair sample of events.

decay signatures. Figures 25–28 show the distributions for $e^+e^-\pi^+\pi^-$, $e^+e^-\pi^+\pi^-\pi^0$, $e^+e^-\pi^+\pi^0$, and $e^+e^-\pi^-\pi^0$, which are sensitive, respectively, to $T^0\rightarrow\gamma_v\rho$, $T^0\rightarrow\gamma_v\omega$, $A_2^+\rightarrow\gamma_v\rho^+$, $A_2^-\rightarrow\gamma_v\rho^-$, where T^0 is f^0 or A_2. In each of these cases, the background samples closely resemble the data and we find no evidence for radiative decays of either A_2 or f^0. We have also examined the final states

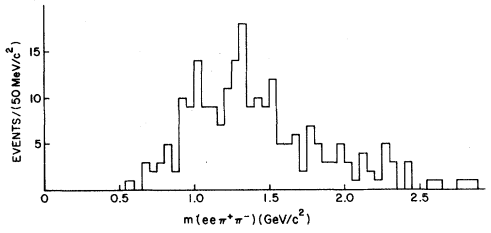

FIG. 25. Effective-mass distributions for $e^+e^-\pi^+\pi^-$ combinations taken from the anomalous-pair sample of events.

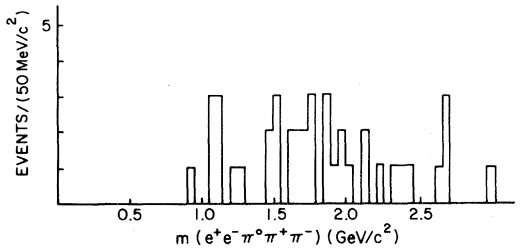

FIG. 26. Effective-mass distributions for $e^+e^-\pi^0\pi^+\pi^-$ combinations taken from the anomalous-pair sample of events.

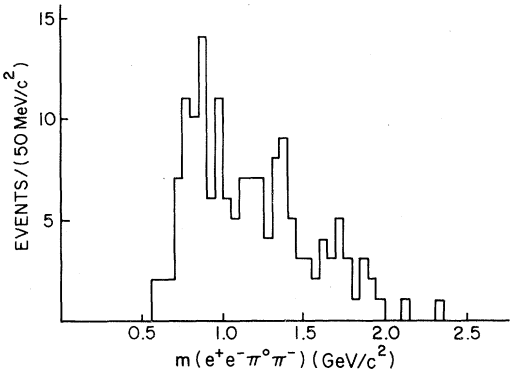

FIG. 28. Effective-mass distributions for $e^+e^-\pi^0\pi^-$ combinations taken from the anomalous-pair sample of events.

$e^+e^-\gamma\pi^\pm$, $e^+e^-\gamma\pi^+\pi^-$ with no narrow resonance seen; the upper limits on the fraction of anomalous pairs contributed by any *narrow* state for the various final states are summarized in Table III.

We have examined the possibility that the production mechanism is E^+E^- with $E^\pm\to e^\pm\gamma$ by examining the scatterplot of $M(e^+\gamma)$ vs $M(e^-\gamma)$. No enhancement is observed. We thus rule out the possibility of heavy electrons; however, this analysis would not be sensitive to the production of supersymmetric partners of the electrons owing to the low detection probability for the resulting photino in $S^\pm\to e^\pm\tilde{\gamma}$.

Because of the similarity of the shapes of the anomalous pair mass and p_T distributions to those for η,ω internal conversion pairs, we have pursued a suggestion[13] that the anomaly may arise from a production of a broad (nonresonant) $J^P=0^-$ state with subsequent $e^+e^-\gamma$ decay. This implies that the anomalous pairs should be associated with a single γ. The effective-mass distribution for e^+e^- (Fig. 23) is not itself inconsistent with this hypothesis. We have studied the associated photon multiplicities for the anomalous and other event samples to look for this effect. Photons were defined, as before, as energy clusters in the BSD unaccompanied by an entering charged track. The minimum acceptable energy for a photon was 0.2 GeV.

There is a background to the photon sample due to bremsstrahlung by the trigger e^+ and e^- in the target and the MPS chambers. We have calculated that 29% of the events should have a radiated photon in the BSD with energy exceeding 0.2 GeV. Since this fraction drops rapidly with E (to 10% for $E_\gamma>0.5$ GeV and 2% for $E_\gamma>1$ GeV), we have studied the associated photon multiplicities at several photon energy cuts. Survival fractions of photons from π^0,η Dalitz decays are weakly dependent on the energy threshold (80% for $E_\gamma>0.5$ GeV

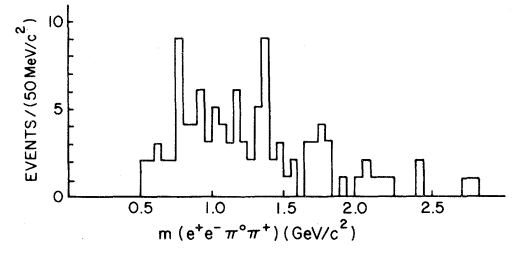

FIG. 27. Effective-mass distributions for $e^+e^-\pi^0\pi^+$ combinations taken from the anomalous-pair sample of events.

TABLE III. Anomalous-source branching-ratio upper limits

Final state	% of anomaly (upper limit)
$e^+e^-\pi^0$	7±7
$e^+e^-\pi^+$	3±3
$e^+e^-\pi^-$	8±4
$e^+e^-\gamma\pi^+$	4±4
$e^+e^-\gamma\pi^-$	$3\pm^{5}_{3}$
$e^+e^-\gamma\pi^+\pi^-$	7±6
Tensor-meson channels	
$e^+e^-\pi^+\pi^-$	6±4
$e^+e^-\pi^0\pi^+\pi^-$	2±2
$e^+e^-\pi^0\pi^+$	5±4
$e^+e^-\pi^0\pi^-$	10±5
$e^+e^-\gamma$ $(m\approx m_\eta)$	Consistent with η background expected

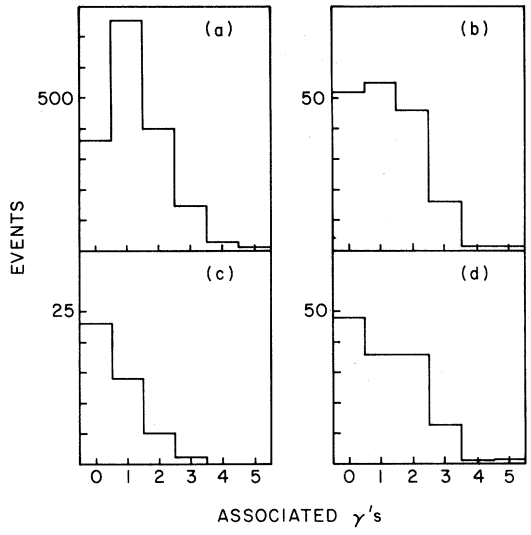

FIG. 29. Distributions of the number of associated γ's observed for various electron pair m and x intervals. (a) $m<0.1$ GeV/c^2 and $x<0.5$, (b) $0.1\leq m<0.6$ GeV/c^2 and $x\leq 0.5$, (c) $m\geq 0.6$ GeV/c^2 and $x\geq 0.7$, (d) $0.1\leq m<0.6$ GeV/c^2 and $x\leq 0.5$ after subtracting the contributions from η and ω internal conversions.

and 72% for $E_\gamma>1$ GeV). Our conclusions presented below do not depend upon the precise threshold for photon energy; we here present data for $E_\gamma>0.5$ GeV.

Figure 29 shows the distribution of number of photons, n_γ, per event for several categories of events. Figure 29(a) shows the n_γ distribution for $m<0.1$ GeV/c^2 and $x<0.5$. These events are almost wholly π^0 Dalitz decays or close conversions and thus should have at least one photon present. For this sample, $n_\gamma=0$ occurs only through detection inefficiency. The computed fraction of γ's hitting the BSD with $E_\gamma>0.5$ GeV for π^0 Dalitz decays is 80%; overlaps of these γ's with charged tracks and leakage of showers between the upper and lower halves of the BSD will reduce this somewhat. The measured fraction, f_0, of events showing zero photons for this Dalitz sample is 0.214 ± 0.010. Figure 29(b) shows the distribution for the anomalous event region $0.1\leq m\leq 0.6$ GeV/c^2 and $x<0.5$. We observe a larger fraction of the events in which $n_\gamma=0$ than for the π^0-Dalitz-decay sample; $f_0=0.304\pm0.035$. When the n_γ distribution in this region is corrected for the contamination due to η and ω internal conversions, we find $f_0=0.359\pm0.042$ for the anomalous events alone. The distribution in n_γ for this subtracted anomalous sample is shown in Fig. 29(d). Figure 29(c) shows a comparison distribution taken from a sample $m\geq 0.6$ GeV/c^2 and $x\geq 0.7$ which is dominantly the direct decays of $\rho,\omega\rightarrow e^+e^-$. Here $f_0=0.525\pm0.076$ shows a strong tendency for no additional photons in these events. This is expected since there are no photons from the ρ,ω decay itself and the large x of production causes the associated π^0 production to be small.

We conclude from these associated multiplicity distributions that the anomalous pairs are not always produced in an $e^+e^-\gamma$ configuration. The n_γ distribution in the anomaly is in fact similar to that seen in unbiased events. We have checked this in our data by identifying and removing the γ from $\pi^0\rightarrow\gamma e^+e^-$ in our low-mass sample, and plotting the n_γ distribution of the *remaining* photons. The energy distribution of these remaining photons also conforms to what we observe for photons associated with anomalous pairs. The situation is also confirmed by our study of the associated-charged-particle multiplicities, for which anomalous and Dalitz samples show statistically identical distributions. The ρ,ω direct decay sample shows the same increase in the fraction of events with zero associated hadrons as was seen above for associated photons.

V. DISCUSSION

The electron-pair anomaly reported here is in agreement with several other recent experiments studying low-mass dileptons. Our experiment is, in addition, capable of detecting both charged particles and photons produced in association with the e^+e^-. In this section, we comment upon the inferences to be drawn from the observed anomaly and discuss the possible sources of this effect.

A major motivation for searching for dilepton anomalies was the reported existence of anomalous single electron production near $x=0$.[2-5] The available single-lepton measurements in the 10—20-GeV region were not in agreement[6]; it is thus most interesting to try to infer single-electron yields from the observed dielectron measurements. The bulk of the single-electron experiments have been performed near $x=0$, whereas dilepton measurements are all in the range $x>0.1$. It is necessary to make some assumptions on the x and p_T dependences of dielectrons in order to extrapolate to $x=0$.

Although the dielectron anomaly is similar in this experiment and that of Ref. 13, there is a difference in absolute magnitude of about a factor of two. For the purpose of estimating single electrons due to the electron-pair anomaly, we make the following assumptions consistent with *both* experiments:

(a) $d\sigma/dx=(6\ \mu\text{b})e^{-6|x|}$ for $0.2\leq m\leq 0.6$

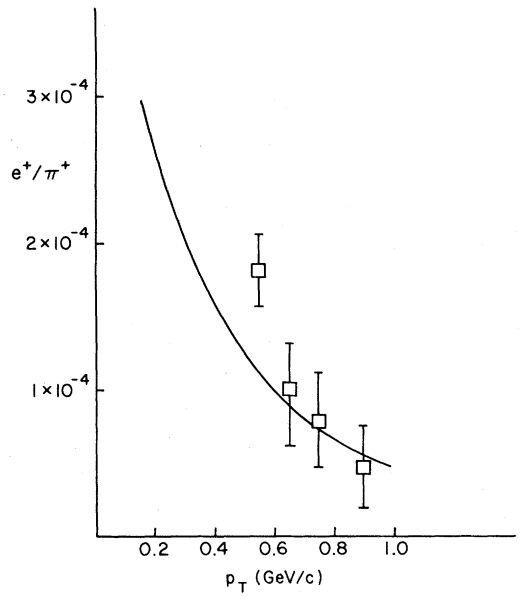

FIG. 30. Predicted contribution to the e^+/π^+ ratio at $x=0$ versus p_T from this experiment (solid curve). The data points are taken from Ref. 4 and are for $\pi^+ p$ and pp collisions at 15 GeV/c and $x=0$.

GeV/c^2 (we assume symmetric production in forward and backward hemispheres).

(b) $d\sigma/dp_T \propto p_T e^{-6.5p_T^2}$.

(c) $d\sigma/dm \propto 1/m$ for $m \gtrsim 0.1$ GeV.

(d) $d\sigma/d\cos\theta$ is the same as the angular distribution of electrons from π^0, η internal conversions: i.e., approximately $(1+\cos^2\theta)$.

From these cross sections and decay distributions, we have computed the cross sections for single e^+ or e^- production within specific Δx and Δp_T intervals for $0.1 \le m \le 0.6$ GeV/c^2. The lower mass limit is that stated by the best statistics experiment observing single electrons[4] as the experimental lower limit for yielding the anomaly in their experiment. To compare these results with the published e/π ratios, we divide the single-electron cross sections by the inclusive π^+ production cross sections. These are taken to be equal to the values given for inclusive π^- production in $\pi^+ p \to \pi^- X$ at 16 GeV/c.[27]

The resulting $e^\pm/\pi^\pm$ ratios predicted for $\pi^- p$ collisions at 17 GeV/c are shown in Fig. 30 for the interval $-0.1 \le x \le 0.1$. The solid line is our calculated rate based on anomalous pairs above 0.1 GeV/c^2 in mass. It is uncertain to within a factor two due to errors on both e^+e^- and π^+ inclusive cross sections and also to uncertainties in the extrapolation procedure to backward hemisphere e^+e^- production. The data points are those of Ref. 4 for e/π^+ at $x=0$ in 15-GeV/c pp and $\pi^+ p$ collisions. The agreement is good and we conclude that the single-electron signal is adequately explained in terms of our anomalous e^+e^- production. Our predicted e/π values agree well with Beier *et al.*[4] as shown. They lie below the reported e/π values from 13 GeV/c pp collisions of Maki *et al.*[5] at $p_T > 0.4$ GeV/c and are above the e/π ratio reported by Makdisi *et al.*[6] for 12-GeV/c pp collisions above $p_T = 0.3$ GeV/c.

The same calculation reported above based on the observed e^+e^- production gives predicted e/π ratios falling as x increases. For $0.4 \le p_T \le 0.6$ GeV/c, and e/π ratio is computed to be 1.4×10^{-4}, 0.7×10^{-4}, and 0.35×10^{-4} for the x intervals $-0.1 \le x \le 0.1$, $0.1 \le x \le 0.3$, and $0.3 \le x \le 0.5$, respectively.

The observation of unexplained lepton-pair production at masses $0.2 \le m \le 0.6$ GeV/c^2 leads naturally to the question of direct real-photon production. Direct single photons have been observed at high energies and large p_T,[16] and have also been seen[17,18] in 10.5-GeV/c $\pi^+ p$ collisions at very low x and p_T. Limits on γ/π have been set[19] at moderate p_T in 24-GeV/c pp collisions at less than 15%. Since we have observed anomalous e^+e^- production in this experiment we are tempted to hypothesize that these pairs form a continuum connecting to real photons in the standard way. Under such assumptions we can deduce expected values for γ/π and confront these with available experimental information.

The mass distribution for internal conversion of photons can be related to the photon cross section, to first order in α by[28]

$$\frac{d^2\sigma(ee)}{dm\,dx} = \frac{2\alpha}{3}\left[1+\frac{2\mu^2}{m^2}\right]\left[1-\frac{4\mu^2}{m^2}\right]^{1/2} \times \frac{1}{m}\left[1-\frac{m^2}{M^2}\right]\frac{d\sigma(\gamma)}{dx}$$

after integration over p_T. Here, μ is the electron mass, m is the e^+e^- pair mass, and M is the available energy (Q value) in the case that the photons come from a specific particle decay (e.g., π^0,η,ω internal conversions). We have ignored here the possibility of abnormal polarization states for virtual photons giving rise to a mass-dependent structure function, and a kinematic factor $=\beta^*(e^+e^-)$ which is essentially one in our kinematic regime. Both of these effects were included in a previous analysis[13] and found to be relatively unimportant.

As discussed in Sec. IV, the anomalous electron-pair cross section in this experiment has been found to be well represented by

$$\frac{d\sigma}{dx}=(3.9\pm1.4)\mu b e^{-(5.5\pm0.7)x}$$

after integration over all p_T and over the mass interval $0.2\leq m\leq 0.6$ GeV/c^2. The mass dependence is consistent with the virtual-photon distribution given above, but is inadequate for making clear determination of the functional form. Therefore to perform the necessary extrapolation to cross sections for low-mass pairs ($m\gtrsim 2\mu$) or for real photons, we explicitly adopt the *assumption* that the mass distribution conforms to the expression above. There remains still an additional assumption to be made on the value of the available energy, M. Since in many respects anomalous pairs are similar to η Dalitz pairs, it is sensible to take $M\approx m_\eta$. A similar proposal was made by Blockus *et al.*,[13] who suggested a broad pseudoscalar parent state for the anomaly, centered at 0.4 GeV/c^2. An extreme alternate choice is $M=\infty$; this latter choice was that actually adopted by Blockus *et al.* in estimating γ/π. Here we present the extrapolation to γ/π for both choices $M=m_\eta$ and $M=\infty$.

We have computed the expected γ/π^+ ratios in $\pi^- p\to(\gamma,\pi)+x$ using extrapolated photon cross sections as outlined above and π^+ inclusive cross sections taken from bubble-chamber measurements of $\pi^+ p\to\pi^- +x$.[27] We find no significant variation in γ/π^+ ratios expected over the whole forward hemisphere $x\geq 0$. The γ/π^+ ratio is about 13% if we assume $M=m_\eta$ and is about 3% if we assume $M=\infty$. Thus we predict (γ/π^+) to be $8\pm5\%$ in 17 GeV/c πp collisions if the connection between massive e^+e^- and real photons follows the standard internal conversion prescription. The error of course is due to the uncertainty in the phase-space cutoff factor.

Such a (γ/π) ratio seems to be rather large, based on a naive expectation that $(\gamma/\pi)\sim\alpha\simeq\frac{1}{137}$. We may note in passing that at high energies (and large p_T) (γ/π) is found to be approximately equal to $x_T=(p_T/p_T^{\max})$. In our experiment, the average x_T is about 0.15, so in fact our extrapolation suggests that direct-photon production at low energies has the same behavior.

It is entirely possible that the extrapolation to zero mass made above is incorrect. The mass distribution of anomalous e^+e^- pairs could go to zero (or fall below a m^{-1} extrapolation) if such pairs were associated mainly with longitudinally polarized photons, or if the parent state of such pairs were cut off at low mass. It is thus interesting to look for any indication of direct photons in the 10–20-GeV/c region. There have been searches for real photons[17] and for low-mass ($2\mu\leq m\leq 0.02$ GeV) electron pairs[18] in bubble chambers in this energy range. Both of these experiments have isolated evidence for hadronic bremsstrahlung, consistent with theoretical prediction. The resulting photons or pairs are confined to very low x ($|x|\leq 0.02$) and small p_T ($p_T\leq 20$ MeV/c) and clearly do not explain the higher-mass ($m>0.2$ GeV/c^2) anomaly with its broader x and p_T distribution. The observed[18] low-mass e^+e^- pairs at larger x and p_T agree to within $\pm25\%$ with the expected number from Dalitz decays of π^0 (and η,ω). They can thus not rule out γ/π ratios of order 10%; a determination of γ/π ratios at the 1% accuracy level would clearly help our understanding of the underlying production mechanism.

We turn now to investigate possible dynamical mechanisms of anomalous electron-pair production. The dependence of e^+e^- production found in this experiment and related studies[10,13] show p_T and mass dependences similar to that expected for pairs from η and ω Dalitz decays. The x dependence is somewhat more central than η and ω Dalitz pairs; it is, in fact, rather similar to that for e^+e^- from π^0 Dalitz decay. These observations have led previous workers[13] to hypothesize a broad continuum of pseudoscalar mesonic states, in the range 0–0.8 GeV/c^2 with subsequent partial decay widths into $e^+e^-\gamma$ or $\mu^+\mu^-\gamma$. The integrated cross section of such states would necessarily be several times that for η production. A necessary consequence of this hypothesis is that anomalous e^+e^- pairs will be accompanied by a photon with $m(ee\gamma)$ in the mass range 0–0.8 GeV/c^2. This experiment, with its good efficiency for γ and charged-particle detection, has studied this possibility. The $e^+e^-\gamma$ mass distribution, shown in Fig. 23, is in qualitative agreement with this hypothesis. However, our measurements of associated photon multiplicities, discussed in Sec. IV and summarized in Fig. 29, show no evidence for enhanced photon production in anomalous pair events. After subtracting background (Dalitz) events, the anomalous events show similar photon multiplicities as do unbiased triggers. The fraction of anomalous events showing zero associated photons is 3.4 standard deviations higher than what is seen in events with known Dalitz pairs. We stress that our photon-detection probability is high (e.g., 79% for $\eta\to e^+e^-\gamma$). The probability for detecting the γ in a Dalitz-type decay is only weakly dependent upon the x of the observed e^+e^- pair for $x\lesssim 0.7$ where the anomaly is strong. Thus we conclude that an explicit $e^+e^-\gamma$ mechanism cannot explain all of the dielectron anomaly.

We have investigated the possibility that various known mesons could be responsible for the lepton pairs. A previous dimuon experiment investigated this possibility in $\mu^+\mu^-$ charged hadron final states

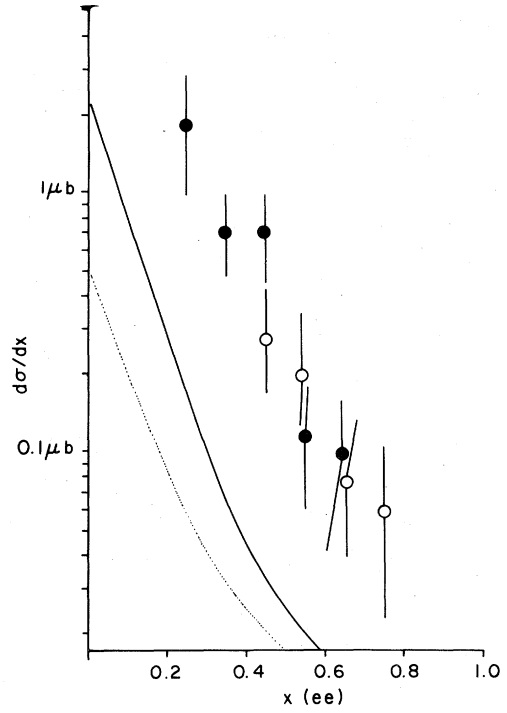

FIG. 31. Anomalous-electron-pair inclusive cross sections as a function of x for this experiment; closed circles are for trigger PAIR A and open circles are for PAIR B. The solid curve is a calculation of the Drell-Yan process using structure functions with scaling from Ref. 35 (and an enhancement factor of 2.06). The dotted curve is the calculation using nonscaling structure functions.

and concluded that no single-particle decay accounted for the effect. In this experiment, we have also examined final states involving π^0's or γ's. Our conclusion is that no single radiative decay of a known particle contributes more than 8% of the observed dielectrons. In particular, radiative decays of A_2 or f mesons (into e^+e^- plus vector meson) can account for no more than 25% of all anomalous pairs. While it is possible that one could account for perhaps half of the anomalous pairs by summing over all of our upper limits for such radiative decays of known particles, we found no positive evidence for this kind of explanation. Existing cross sections and presumed branching ratios confirm the conclusion that known states, apart from $\eta\to e^+e^-\gamma$ and $\omega\to e^+e^-\pi^0$, contribute little to massive-electron-pair cross sections.

Production of electron pairs could proceed by an analog of the two-photon mechanism observed in e^+e^- collisions. We have computed the contribution for the two-photon diagram for quark-quark scattering, summed over valence quarks within the incident π^- and p. We obtain a cross section of approximately 15 nb at our energy which is of the order 2% of the observed anomaly. We do observe two events consistent with the reaction $\pi^-p\to e^+e^-\pi^-p$. The two-photon process is not a major contributor to anomalous electron pairs.

The early measurements of single-lepton production were surprising because they exceeded expectations from such sources as known meson decays and Drell-Yan[7] production by about an order of magnitude. The pair production confirms this result. The Drell-Yan mechanism is presumed to be a valid picture for massive pair production, since the corresponding short-distance interaction permits the validity of the underlying impulse approximation. Indeed massive-pair production rates agree to within a factor of two of prediction,[34] with possible improvements after including various QCD corrections. We have computed the Drell-Yan process contribution to electron-pair production for $0.2\leq m\leq 0.6$ GeV/c^2, integrated over all p_T. We have used structure functions taken from recent data on deep-inelastic lepton scattering[35] and have included an enhancement (K factor) of 2.06. Figure 31 shows this calculation, together with our data, presented as a function of x. Although such a calculation should not be taken too seriously (it invokes the proton structure function at Bjorken x very near zero), it does indicate that our lepton pairs are produced a factor of ten more copiously than expected from the dominant high-mass mechanism.

A similar conclusion was drawn by Bjorken and Weisberg[36] on the basis of single e/π ratios and led them to propose an enhancement mechanism for the Drell-Yan process. They observed that in hadron-hadron collisions, many quarks (and antiquarks) are produced at rather low relative momenta, and that annihilations between this larger sample of *produced* quarks would give an order-of-magnitude enhancement in observed dileptons.

Some elaboration and modification of this idea has occurred. Computation of the dilepton production distributions in m, x, and p_T (Ref. 37) gave some discrepancies with experiment when the assumption was made that all pairs proceed through $J^{PC}=1^{--}$ (virtual-photon) intermediate states. Some additional mechanism seems required, as provided, for example, by soft-gluon radiation terms.[37] The same kind of arguments—in particular, the difficulty in reproducing the low $\langle p_T{}^2\rangle$ observed with a $q\bar{q}\to\gamma_v\to e^+e^-$ mechanism—led to the hypothesis[13] that $q\bar{q}\to\gamma\gamma_v\to\gamma e^+e^-$ is the primary mechanism. Qualitatively, the low-mass pair production data appear to require the increase in cross

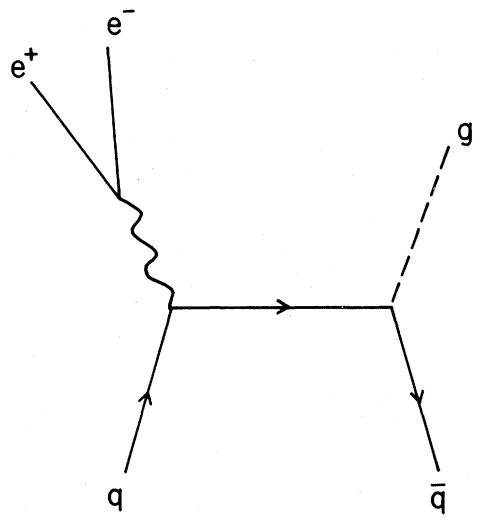

FIG. 32. Diagram for anomalous-electron-pair production involving virtual-gluon radiation.

section afforded by inclusion of partial waves other than $J^P=1^-$. The p_T and x distributions are in better agreement with data when there is radiation of a light quantum (photon or gluon) in the annihilation of quark-antiquark. In this experiment, we rule out a mechanism in which a photon is radiated in most of the anomalous pair events, but are in good qualitative agreement with the notion that gluon radiation in the annihilation plays a dominant role. We have in mind a diagram such as shown in Fig. 32, where the radiated gluon remains to be absorbed in the evolving hadronic materialization.

A mechanism such as proposed, involving the Drell-Yan process and its large QCD corrections in the evolving hadronic state appears to be similar to models couched in a thermodynamic language.[38] This model appears to be in agreement with the main conclusions of our experiment regarding the structure of the final state containing anomalous electron pairs; that is, it would naturally predict little difference in multiplicity, effective masses or particle content when compared with ordinary events. Anomalous pairs arise as a radiative electromagnetic effect superimposed on all the normal hadronic subprocesses available in the collision. The excess of such events occurs only because one has to allow for radiation from all final-state quark charges.

In this picture for anomalous lepton production, it is natural to predict that the ratio of lepton pairs to hadrons should be essentially independent of kinematic details, incident-particle type, or the energy of the collision. So far as we know, this is consistent with the data on hadronic production of both leptons pairs and single leptons. Experiments with pion and proton beams, on proton or nuclear targets, at energies from 10 to 1500 GeV in both small- and large-x regions have seen similar lepton to hadron ratios. It is also expected that experiments in which excited hadronic states are produced by nonhadronic projectiles (e.g., photoproduction, deep-inelastic lepton scattering, or e^+e^- collisions) should exhibit the same ratio of dilepton production. There are two pieces of evidence that this is the case. The first was the study of photoproduced dimuons of mass below 0.6 GeV/c^2 at energies $8.5 \leq E_\gamma \leq 11.7$ GeV.[39] The observed dimuons exceeded the known contributions by a factor of about 10 over the range $2 \leq q^2 \leq 6$ and $1.5 \leq \nu \leq 6.5$. The second confirmation comes from deep-inelastic neutrino scattering,[40] in which trimuon production is observed at levels exceeding that expected for charged-current events with associated charmed-particle production or standard Bethe-Heitler pairs. There appears[41] to be a component of $\mu^+\mu^-$ production from the hadronic vertex with characteristically low dimuon mass. The size of this signal is larger than known electromagnetic processes by a factor of about three. Searches for anomalous dilepton production in e^+e^- collisions have been hampered to date by inadequate statistics.

In conclusion, we find that anomalous electron pairs are produced in π^-p collisions at 17 GeV/c. Known decays such as $\eta \to \gamma e^+e^-$ and $\omega \to \pi^0 e^+e^-$ are insufficient to explain the events above $m=0.2$ GeV/c^2. Production is dominantly at low x and low p_T. There is no evidence for particular radiative decays of known resonances. There is no enhancement over ordinary events in associated photon or charged-particle production. Our results are in agreement with a mechanism of production in which a virtual photon is radiated from internal quark charges (including those produced in the collision) in association with other light quanta (e.g., gluons), together with annihilation of these quark-antiquark pairs.

ACKNOWLEDGMENTS

We take this opportunity to express our appreciation to the members of the Multiparticle Spectrometer Facility at Brookhaven whose help in running this experiment was essential. We are appreciative of help in the early phases of the experiment from Dr. S. Moore and Dr. P. Schmidt. The contributions of J. Mayman, J. Scheliga, E. Hassel, and T. Regan were essential in constructing the apparatus for the experiment. Conversations with Dr. W. Dunwoodie and Professor J. Smith have been most useful in our understanding of the data.

*Present address: Computer Science Corporation, Silver Spring, MD 20910.
†Present address: Syracuse University, Syracuse, NY 13210.
‡Present address: Bell Laboratories, Murray Hill, NJ.
§Permanent address: University of Cincinnati, Cincinnati, OH 45221.
**Present address: Bell Laboratories, Holmdel, NJ 07733.
††Present address: Recon, Watkins-Johnson Co., San Jose, CA 95131.
‡‡Present address: Kaman Sciences Corporation, Colorado Springs, CO 80933.

[1]Reviews of high-p_T direct-lepton production are contained in L. M. Lederman, Phys. Rep. 26C, 149 (1976) and N. S. Craigie, *ibid.* 47C, 1 (1978).
[2]L. Baum *et al.*, Phys. Lett. 60B, 485 (1976).
[3]M. Barone *et al.*, Nucl. Phys. B132, 29 (1978).
[4]E. W. Beier *et al.*, Phys. Rev. Lett. 37, 1117 (1976).
[5]A. Maki *et al.*, Phys. Lett. 106B, 423 (1981).
[6]Y. Makdisi *et al.*, Phys. Rev. Lett. 41, 367 (1978).
[7]S. Drell and T. M. Yan, Phys. Rev. Lett. 24, 181 (1970); 25, 316 (1970); Ann. Phys. (N.Y.) 66, 578 (1971).
[8]K. J. Anderson *et al.*, Phys. Rev. Lett. 37, 799 (1976).
[9]D. M. Grannan *et al.*, Phys. Rev. D 18, 3150 (1978).
[10]K. Bunnell *et al.*, Phys. Rev. Lett. 40, 136 (1978); B. Haber *et al.*, Phys. Rev. D 22, 2107 (1980).
[11]J. Ballam *et al.*, Phys. Rev. Lett. 41, 1207 (1978).
[12]R. Stroynowksi *et al.*, Phys. Lett. 97B, 315 (1980).
[13]D. Blockus *et al.*, Nucl. Phys. B201, 197 (1982).
[14]J. Stekas *et al.*, Phys. Rev. Lett. 47, 1686 (1981).
[15]S. Mikamo *et al.*, Phys. Lett. 106B, 428 (1981).
[16]M. Diakonov *et al.*, Phys. Lett. 87B, 292 (1979); 91B, 296 (1980); C. Kourkemelis *et al.*, Nucl. Phys. B179, 1 (1981); E. Anassontzis *et al.*, Z. Phys. C 13, 277 (1982); A. L. S. Angelis *et al.*, Phys. Lett. 94B, 106 (1980).
[17]A. T. Goshaw *et al.*, Phys. Rev. Lett. 43, 1065 (1979).
[18]A. T. Goshaw *et al.*, Phys. Rev. D 24, 2928 (1981).
[19]E. W. Beier *et al.*, Phys. Rev. Lett. 37, 1114 (1976).
[20]J. R. Elliot *et al.*, Phys. Rev. D 17, 83 (1978).
[21]E. Platner *et al.*, in *Proceedings of the International Conference on Instrumentation for High Energy Physics, Frascati, 1973,* edited by Stanislao Stipcich (Laboratori Nazionali del Comitato Nazionale per l'Energie Nucleare, Frascati, 1973), p. 672.
[22]G. Abshire *et al.*, Nucl. Instrum. Methods 164, 67 (1979).
[23]R. Bosshard *et al.*, Nucl. Instrum. Methods 130, 365 (1975).
[24]E. D. Platner *et al.*, Nucl. Instrum. Methods 140, 549 (1977).
[25]N. N. Biswas *et al.*, Phys. Rev. D 10, 3579 (1974).
[26]The apparent mass of the ρ,ω peak in Fig. 10(a) is below the accepted value by about 8%. We have computed that this shift is what is expected due to the radiative energy loss of the electrons in the hydrogen target.
[27]J. Bartke *et al.*, Nucl. Phys. B107, 93 (1976); M. Deutschmann *et al.*, *ibid.* B103, 426 (1976).
[28]B. E. Lautrup and J. Smith, Phys. Rev. D 3, 1122 (1971).
[29]J. Bartke *et al.*, Nucl. Phys. B118, 360 (1977).
[30]R. L. Kelley *et al.*, Rev. Mod. Phys. 52, S1 (1980).
[31]W. Morse *et al.*, Phys. Rev. B 18, 3145 (1978).
[32]M. Kasha *et al.*, Phys. Rev. Lett. 36, 1007 (1976).
[33]I. H. Dunbar, Phys. Rev. Lett. 41, 210 (1978).
[34]See, for example, J. Lefrancois, in *High Energy Physics—1980,* proceedings of the XXth International Conference, Madison, Wisconsin, edited by L. Durand and L. G. Pondrom (AIP, New York, 1981), p. 1318.
[35]We take the nucleon structure function from the deep-inelastic neutrino scattering [A. Para, in *Proceedings of the 1979 International Symposium on Lepton and Photon Interactions at High Energies, Fermilab,* edited by T. B. W. Kirk and H. D. I. Abarbanel (Fermilab, Batavia, Illinois, 1980), p. 343]. The pion structure function is from Drell-Yan production by $\pi^{\pm}$ [D. DeCamp in *High Energy Physics—1980,* (Ref. 34), p. 149].
[36]J. D. Bjorken and H. Weisberg, Phys. Rev. D 13, 1405 (1976).
[37]V. Černý *et al.*, Phys. Rev. D 24, 652 (1981).
[38]E. V. Shuryak, Phys. Lett. 78B, 150 (1978).
[39]J. F. Davis *et al.*, Phys. Rev. Lett. 29, 1356 (1972); D. O. Caldwell *et al.*, *ibid.* 33, 868 (1974).
[40]T. Hansl *et al.*, Nucl. Phys. B142, 381 (1978); J. G. H. de Groot *et al.*, Phys. Lett. 85B, 131 (1979).
[41]J. Smith, Nucl. Phys. B157, 45 (1979); Phys. Lett. 85B, 124 (1979).